MicroCT scanner performance and considerations for vascular specimen imaging

Michael Marxen
Sunnybrook & Women's College Health Sciences Centre, Department of Medical Biophysics, University of Toronto, Toronto, Canada

Michael M. Thornton
General Electric Medical Systems, London, Canada

Cameron B. Chiarot
Princess Margaret Hospital/University Health Network, Departments of Radiation Oncology, Clinical Physics, and Radiation Medical Physics, Toronto, Canada

Giannoula Klement
Dana-Farber Cancer Institute, Pediatric Hematology/Oncology & Children's Hospital Vascular Anomalies Clinic, Boston, Massachusetts

Janet Koprivnikar
Department of Zoology, University of Toronto, Mississauga, Canada

John G. Sled
Hospital for Sick Children/Mouse Imaging Centre, Department of Medical Biophysics, University of Toronto, Toronto, Canada

R. Mark Henkelman
Sunnybrook & Women's College Health Sciences Centre, Hospital for Sick Children/Mouse Imaging Centre, Departments of Medical Biophysics and Medical Imaging, University of Toronto, Toronto, Canada

(Received 27 May 2003; revised 12 November 2003; accepted for publication 13 November 2003; published 23 January 2004)

Obtaining three-dimensional geometrical data of vascular systems is of major importance to a number of research areas in medicine and biology. Examples are the characterization of tumor vasculature, modeling blood flow, or genetic effects on vascular development. The performance of the General Electric Medical Systems MS8 microCT scanner is examined in the context of these applications. The system is designed to acquire high-resolution images of specimens up to 5 cm in diameter. A maximum resolution of 38 lp/mm at the 10% modulation transfer function level or 22 μm full width at half maximum of the plane spread function can be achieved with 8.5 μm voxels and a 17 mm field of view. Three different contrast agents are discussed and applied for imaging of small animal vasculature: corrosion casting material Batson's No. 17 with an added lead pigment, silicon rubber MICROFIL MV122, and a suspension of barium sulfate (Baritop) in gelatin. Contrast for all of these agents was highly variable in different vessels as well as within the same vessel. Imaging of PMMA tubing filled with MICROFIL shows that even vessels below 20 μm in diameter are detectable and that diameter estimation of vessels based on thresholding is possible with a precision of 2–3 pixels.
[DOI: 10.1118/1.1637971]

I. INTRODUCTION

Information on the detailed three-dimensional structure of complete vascular systems is desirable, for example to aid in the development of blood flow models[1–3] or to differentiate features of vascular systems in genetic knock-out studies.[4] While it is still unrealistic to contemplate an analysis of all vessels within an organ including capillaries, that are smaller than 10 μm in diameter, recently developed high-resolution x-ray computed tomography systems (microCT) are capable of visualizing extensive vascular networks with limitations in resolution and field of view (FOV). After perfusion of the vasculature with x-ray absorbing agents, three-dimensional digital images can be generated with high contrast, which allows immediate computer processing to segment vessels from the tissue background and extract the branching structure and geometric morphology of the vascular network.

In this article, the performance of an MS8 cone-beam CT[5] system manufactured by General Electric Medical Systems (formerly Enhanced Vision Systems, London, Ontario, Canada) is evaluated. The system is designed for excised tissues such as rodent organs and has a maximum FOV of 5 cm and a detector with 2048×2048 pixels. The system can be used for bone density and trabeculation studies, vascular studies using contrast agents or, in general, examinations of very small structures with high x-ray contrast. The presentation of general performance characteristics of the system is followed by a discussion of the potential and limitations of microCT systems of this type for the analysis of vascular structure. The characteristics of three different contrast

agents are examined. The detectability of very small vessels filled with one of the contrast agents (MICROFIL MV122) and the accuracy of diameter measurements are evaluated based on phantom studies. Finally, images of rodent kidney vasculatures loaded with the different contrast agents are presented for qualitative comparison.

High-resolution CT of vascular structure has been applied with impressive results by researchers, for example, at the Mayo Clinic[6] in Rochester, MN, at the Kawasaki Medical School in Okayama, Japan,[7] and, at somewhat lower spatial resolution, at Marquette University,[8] Milwaukee, WI. Several other approaches to study three-dimensional (3D) vascular architecture are possible, particularly if very high resolution is required. Corrosion casts of vascular networks are commonly analyzed using scanning electron microscopy or optical projections.[9,10] In this case, three-dimensional information can be obtained from stereo projections, but fully three-dimensional, digital data sets are difficult to generate and the data are limited in terms of volume coverage. Confocal microscopy[11] generates 3D, digital data sets, but the limited penetration of light into the tissue as well as contrast issues make this technique difficult to apply to structures as large as centimeters. Another option is the assembly of 3D data sets from 2D histological slices.[12] This technique requires considerable effort for large samples, and precise registration of small structures in adjacent slices is difficult to achieve.

II. MATERIAL AND METHODS

The major components of the microCT are the x-ray source, a rotating stage for the sample in the beam path, and the x-ray detector. In our system, the distance from the source to the detector is 237 mm. The maximum FOV of 5 cm for our prototype MS8 system is slightly larger than specified by GE on the Internet. The x-ray source (Kevex PXS5-925EA) has a tungsten target at a 50° angle to the electron beam and is capable of a range of target voltages from 20 to 90 kVp with a maximum beam current of 0.18 mA and a maximum power of 8 W. According to the tube manufacturer, the x-ray flux in air is 2000 R/h at a distance from the tube window of 305 mm at a tube voltage of 90 kVp and a beam current of 0.09 mA. The size of the focal spot is 6.5 μm at 4W and smaller than 9 μm at 8W. For all reported scans, the beam was filtered through 0.5 mm of aluminum to reduce the fluence of low-energy photons.

The detector converts x-ray photons into visible light that is captured by a CCD chip with 12 bit readout and 2048 by 2048 pixel elements, each with an area of $(14\ \mu\text{m})^2$. A fiberoptic taper is glue-bonded to the CCD surface. The fibers have been stretched from a diameter of 10 μm at the wide end of the taper to 4 μm at the CCD. Use of the taper results in an effective detector area of $(69\ \text{mm})^2$ with $(35\ \mu\text{m})^2$ pixels. A fiberoptic plate coated with cesium iodide (CsI) crystals ($40\ \text{mg/cm}^2$) for x-ray conversion into visible light is bonded to the front face of the taper. The detector is thermoelectrically cooled down from about 40 °C without cooling to 20 °C. Stronger cooling would be possible if air humidity is strictly controlled to avoid condensation.

The rotation stage allows angular increments of 0.1°. Magnification factors from approximately 1.4 to 4 are possible by translating the object along the central ray between the tube and the detector. The whole system is enclosed in a shielded casing and meets x-ray cabinet standards[13] of 0.575 mR/h maximum exposure rate at a distance of 5 cm. Spatial distortions of the projection images are corrected by an unwarping procedure.

Pixel intensities are corrected using dark and bright field images and assuming linear response (with dark field offset) of each pixel to photon fluence. Aberrant pixels are registered in a list and replaced in each projection image using bilinear interpolation of neighboring pixels. Before reconstruction, the Ram–Lak filter[14] is applied to each projection image. Feldkamp's algorithm[5] is used for reconstruction. Projection images can be acquired either distributed over a full circle (360° mode[5]) or spaced over 200° (Parker mode[15]). Exposure times are limited to 2 s per frame due to detector saturation, but higher exposure times can be achieved by averaging multiple frames.

The criteria to evaluate the performance of this high-resolution CT system have been inspired by the quality control recommendation for clinical CT scanners in Report No. 1 of the American Association of Physicists in Medicine (AAPM) ''Phantoms for Performance Evaluation and Quality Assurance of CT Scanners.'' In our evaluation, phantoms and organ samples were scanned in cylindrical, acrylic sample tubes with diameters of 32 or 20 mm. To reduce dynamic range and beam hardening, the tubes were surrounded by a stationary acrylic bath with a bore diameter of 33.5 mm and a thickness of 37 mm along the central ray. For measurements of noise and field flatness, a tightly fitting acrylic cylinder was inserted into the bath for the bright field acquisition. A proprietary algorithm included in the commercial reconstruction software was used to reduce ring artifacts. The following tests were performed:

(i) Resolution limit of the x-ray detector: A 10 μm tungsten wire was placed on the front face of the detector at a slight angle to the vertical pixel columns of the detector in order to measure the line spread function (LSF) and derive the presampled modulation transfer function (MTF) of the x-ray detector. A well-sampled LSF was assembled by sorting the pixel intensity data according to the distance from the estimated center of the wire. The Fourier transform of the LSF is the MTF. The full width at half maximum (FWHM) of the LSF was determined, as well as the 5% and 10% relative intensity values of the MTF.

(ii) Resolution at maximum magnification: A phantom containing a 1.5 mm diameter ruby sphere[16] (supplied by A. Seifert and M. J. Flynn, University of Michigan, Ann Arbor, MI) was scanned at the maximum magnification (4.08) resulting in 8.5 μm voxels in the object plane. Six hundred projections were acquired with an x-ray tube voltage of 80 kVp and an exposure of 288 mAs. The surface spread function (SSF) of the reconstructed sphere was measured and is equivalent to an

edge spread function (ESF) in two dimensions.[16] The derivative of the SSF is the plane spread function (PLSF), which is analogous to the LSF being the derivative of the ESF in two dimensions. In the three-dimensional case, the MTF is the Fourier transform of the PLSF. The calculation of the three-dimensional PLSF and MTF was performed by Seifert.[16]

(iii) Dose efficiency: A sample vial (inner diameter 25 mm) of water was scanned in a sample holder with an inner diameter of 28 mm and an outer diameter of 32 mm. Twelve-hundred views with a total exposure of 4277 mAs were acquired over 360° at 80 kVp and a magnification of 1.39. The scan time to reach an exposure of 4277 mAs is approximately 16 h. The estimated tissue dose at this exposure approaches 4000 Gy, which is far beyond the lethal dose of approximately 6 Gy for a live mouse. Fifty micron isotropic volume elements (voxels) are reconstructed. Total exposures over the range from 396 to 4277 mAs were obtained by skipping views and employing the Parker[15] and 360° methods.[5] The noise (standard deviation of the signal intensity) in water was measured in a 30×30 pixel region of interest (ROI) in an axial slice and quantified in Hounsfield units (HU) as a function of exposure. On the Hounsfield scale, air is assigned a CT number of −1000 HU and water is 0 HU. Different independent sources of noise contribute additively to the variance and in quadrature to the standard deviation. A power law with a quadrature offset was fitted to the standard deviation of the signal as a function of exposure. Curve fitting was performed using ORIGIN 6.1 (Origin Lab Corp., Northampton, MA).

(iv) Effect of voxel size: Using a similar protocol as in (iii) with 600 views and an exposure of 119 mAs, the noise is plotted as a function of voxel size. Isotropic voxels with 50, 100, 200, 250, 400, 500, and 800 μm edge length were reconstructed. The reconstruction is preceded by equivalent binning of pixels in the projection images. A power law with a quadrature offset was fitted to the standard deviation of the data.

(v) Detected quantum efficiency (DQE): The DQE is reported as calculated by Cunningham[17] from acceptance test data for an equivalent detector. The data were acquired at 80 kVp with no object in the beam path.

(vi) Field flatness: A solid acrylic cylinder with a diameter of 31.8 mm was scanned at 80 kVp and 130 mAs at a magnification of 1.39. Images with 250 μm voxels were reconstructed. A profile plot through the center of the cylinder is presented. No additional flattening correction was applied.

(vii) System linearity: Epoxy resin-based tissue mimicking materials with hydroxyapatite densities of 50, 100, 150, 200, 300, 350, 400, and 1030 mg/ml were scanned at 80 kVp and 499 mAs. Samples were manufactured either by CIRS, Norfolk, VA, or by Gammex RMI, Middleton, WI. Sample plugs of approximately 2 mm in diameter were placed at constant radius in a 25 mm diameter acrylic holder in a large sample tube. The mean and standard deviation of the signal in HU was measured for volumes of 20 ×20×20 50 μm voxels. Linear regression was performed.

In addition, we performed a number of experiments to test the capabilities of the system for vascular structure analysis in rodent organs.

(viii) The signal intensity in HU of common contrast agents used in vascular studies was determined. We have used Batson's No. 17 polymethylmethacrylate (PMMA—10 ml base, 1.2 ml catalyst, and 2 drops promoter) with an added lead pigment (approximately 0.1 mg/cc of Flake White No. 2, Winsor & Newton, London, England, containing basic lead carbonate PW1, zinc oxide PW4, and safflower oil) to increase contrast, the silicone rubber injection compound MICROFIL MV-122 (Flow Tech, Inc., Carver, MA—8 ml MICROFIL MV122, 10 ml dilutent and 0.9 ml curing agent) containing lead chromate, and a 40% suspension of the barium sulfate contrast agent Baritop (Kaigen Co., Osaka, Japan) in water plus 5% gelatin.

(ix) To demonstrate the ability of the system to detect small vessels, a section of PMMA tubing filled with MICROFIL contrast agent and oriented parallel to the axis of rotation was scanned at 80 kVp, 810 mAs, and a magnification of 3.2 using 900 different views. The PMMA tubing was embedded in 6% gelatin and mounted in a sample holder with 16 mm inner diameter and 20 mm outer diameter. The reconstructed voxel size was 10.85 μm. An optical microscope was used to acquire digital images with 0.23 μm pixels of the MICROFIL filled tubing at a specific location. From these images, the inner and outer diameter of the tubing was measured. The real inner diameter R_r can be calculated from the apparent inner diameter R_a and the outer diameter R_o taking into account the refractive indices of PMMA ($n_1=1.49$) and air ($n_2=1$)

$$R_r = R_a - \sqrt{R_o^2 - R_a^2}\cdot C,$$

where $C = \tan[\arcsin(R_a/R_o) - \arcsin(n_2 R_a / n_1 R_o)]$.

The inner diameter of the tubing was determined to be 18±2 μm. Lateral cross-sectional microCT profiles are plotted. For comparison, profile plots of a 25 μm aluminum wire are also shown.

(x) For vascular studies, it is important to know how precisely vessel diameters can be determined. For that purpose, a similar phantom as in experiment (ix) using a larger PMMA tube with an inner diameter of 163±3 μm filled with MICROFIL was scanned with the same protocol as in (ix). The optical measurement of diameter was compared with lateral profile plots.

(xi) In our lab, we have examined a number of different experimental procedures and contrast agents. Experi-

TABLE I. Summary of the experimental parameters and results for three kidney specimens.

Experimental procedure			
Contrast agent	Batson's No. 17+lead pigment	MICROFIL MV-122	Baritop in gelatin
Animal	Mouse	Mouse	Rabbit
Injection site	Left ventricle	Left ventricle	Renal artery
Drainage site	Cut in right atrium	Cut in right atrium	Renal vein
Perfusion pressure [mmHg]	120	160	150
Anesthesia	Isofluorane (2% in 11/min oxygen)	Ketamine/Xylazine (i.p. 50/10 mg/kg)	Excised organ
Flushing media	Heparinized saline (1 unit/ml)	Heparinized saline (1 unit/ml)	Heparinized saline (1 unit/ml)
Sample preparation	Tissue macerated in potassium hydroxid and cast scanned in air	Conserved with 10% formalin and embedded in 6% gelatin	Conserved with 10% formalin and mounted in ultrasound gel
Scan parameters			
kVp [keV]	60	80	89
Exposure [mAs]	432	324	864
Magnification	3.2	3.2	1.58
Voxel size [m]	11	11	22
Number of views	900	900	900
Scan time [h]	2	2	4.3
Number of reconstr. voxels [millions]	500	500	3200
Reconstruction time [h]	9	9	58
Results			
Contrast [HU]	(−60)–1500	2500–5000	7000–11 000
Noise standard deviation [HU]	120	250	250

ments have been done with mice, rats, and rabbits. Contrast injections were performed into the left ventricle, into the femoral artery, and into excised organs. Other variants in the experiments were the amount and injection site of Heparin, the flushing medium (heparinized saline, formalin, or none), the anesthesia, the perfusion pressure, and the drainage site. In addition to the three contrast agents described above, we tried different additives, particularly pigments and particulates, to Batson's No. 17 or gelatin as well as different concentrations of Baritop in gelatin. We are presenting here for qualitative comparison examples of three kidney specimens, one for each of the contrast agents described in this article. The experimental procedures are not detailed here and are similar to the ones described in Refs. 18 and 19. The experimental parameters are summarized in Table I. Renderings and central slices are presented. The magnification for all scans was selected to minimize the FOV while still covering the whole organ and width of the sample holder. All animal procedures were approved by the animal care committee of Sunnybrook and Women's College Health Sciences Centre.

III. RESULTS

(i) The FWHM of the detector LSF in Fig. 1(a) is 80 μm or 2.3 pixels. The presampled MTF of the detector [Fig. 1(b)] reaches 11.3 lp/mm at the 5% level of the zero-frequency value at 9.5 line pairs/mm (lp/mm) at the 10% level.

(ii) At the maximum magnification of the system of 4.08, the FWHM of the PLSF is 22 μm or the equivalent of 2.6 detector elements [Fig. 2(a)], and the 5% and 10% MTF levels are 43.5 and 38 lp/mm, respectively [Fig. 2(b)]. These values are slightly worse than expected based purely on the magnification (80 μm/4.08=20 μm). This is due to additional focal spot blur, geometric blur, and reconstruction blur.[16]

(iii) The noise in 50 μm voxels (Fig. 3) drops from 47 HU at 396 mAs to 11.5 HU at 4277 mAs. The best power-law fit with quadrature offset to the standard deviation σ of the data is $\sigma=((30\pm40)+(4\pm2)\cdot10^6\times x^{-1.25\pm0.08})^{1/2}(R^2=0.993)$, where x is the exposure in mAs.

(iv) Noise as a function of voxel size (Fig. 4) drops from 68 HU at 50 μm voxels down to 2 HU at 800 μm voxels. The standard deviation σ of the signal can be fitted by the equation $\sigma=((4.2\pm0.6)+(53\pm3)\cdot10^7\, s^{-2.98\pm0.02})^{1/2}(R^2=0.999)$, where s is the voxel size in μm.

(v) Detected quantum efficiency is plotted in Fig. 5 as a function of spatial frequency. The peak values are 0.22 in the horizontal direction (detector rows) and 0.18 in the vertical direction (detector columns). The expected maximum peak value for 45 mg/cm^2 of CsI and an 80 kVp spectrum was estimated to be 0.24.

(vi) The radial flatness of the signal from an acrylic disk is

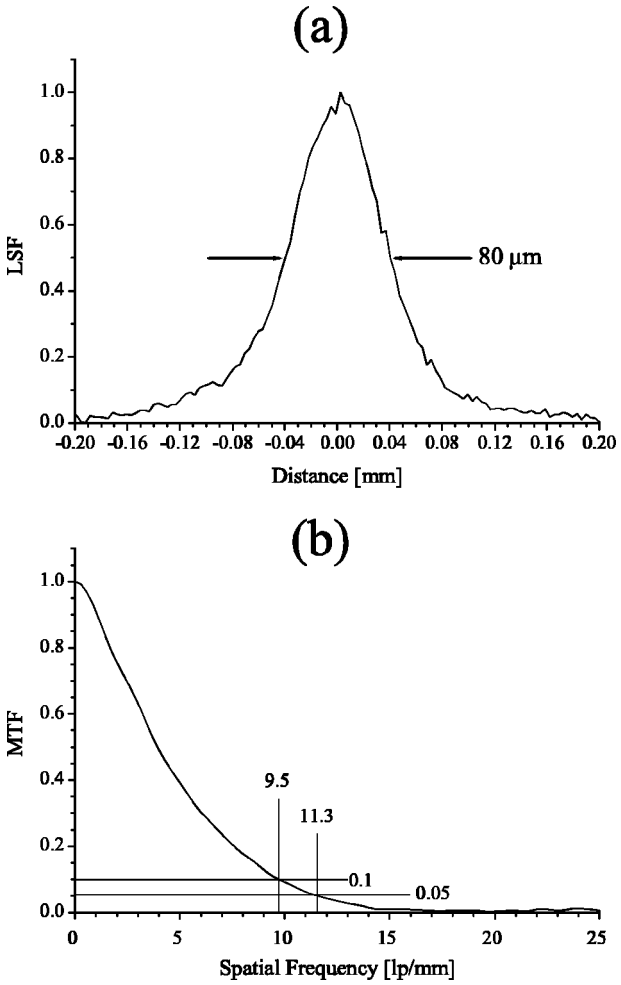

FIG. 1. Line spread function (LSF) and modulation transfer function (MTF) of the x-ray detector. The distance is measured at the front face of the detector with 34.7 μm pixels. The FWHM of the LSF is 80 μm. The 5% and 10% MTF levels are reached at 11.3 and 9.5 lp/mm, respectively.

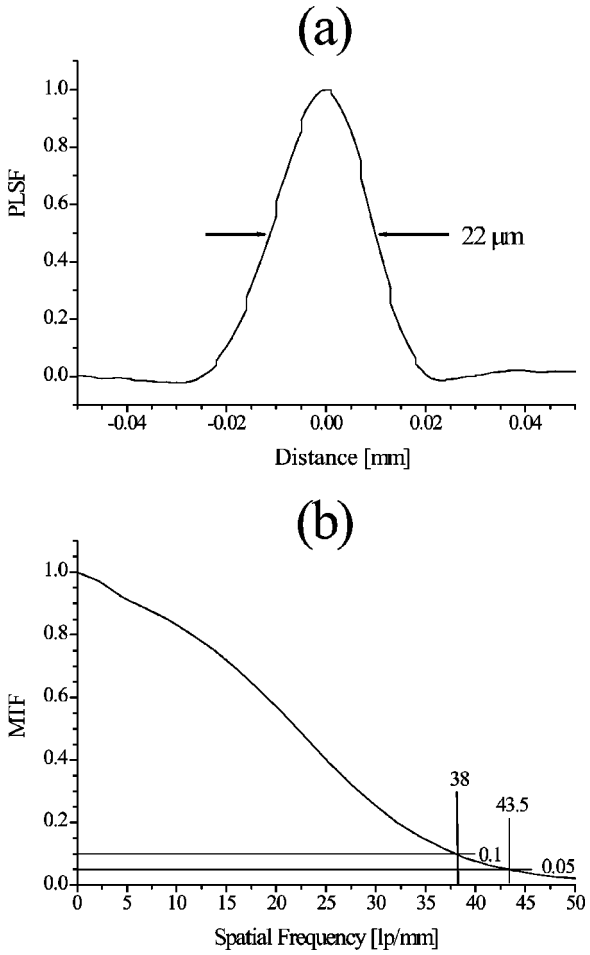

FIG. 2. Plane spread function (PLSF) and MTF for a ruby sphere at the maximum system magnification of 4.08. The distance of the PLSF was measured in the object plane. The FWHM of the PLSF is 22 μm. The 5% and 10% MTF levels are reached at 43.5 and 38 lp/mm, respectively.

shown in Fig. 6. The signal intensity outside of a 3 mm radius varies only between -54 and -64 HU for 250 μm voxels. Ring artifacts due to nonlinear response of individual detector pixels cause a stronger variation in the center from -84 to -53 HU.

(vii) Signal intensity S as a function of hydroxyapatite concentration (Fig. 7) can be fitted with the linear equation $S=(5\pm2)+(2.542\pm0.007)\cdot C$, where C is the hydroxyapatite concentration in mg/cc ($R^2=0.9983$). The maximum deviation of the fit from any data point is 27 HU.

(viii) The contrast for all agents is very heterogeneous within vessels as well as between vessels due to incomplete mixing and settling effects. The contrast in individual vessels ranges from (-60)–1500 HU for Batson's No. 17, 2500–5000 for MICROFIL, and 7000–11 000 HU for Baritop (see Table I).

(ix) The phantom experiment with an 18 μm PMMA tube [Fig. 8(a)] demonstrates that even small vessels filled with MICROFIL can be detected in an ideal case. The FWHM of the signal is approximately 3 pixels (33 μm), which is also approximately the width of the PLSF of the system. The size of the object is smaller than the width of the PLSF, and the peak intensity of the object reaches only 700 HU. For comparison, the

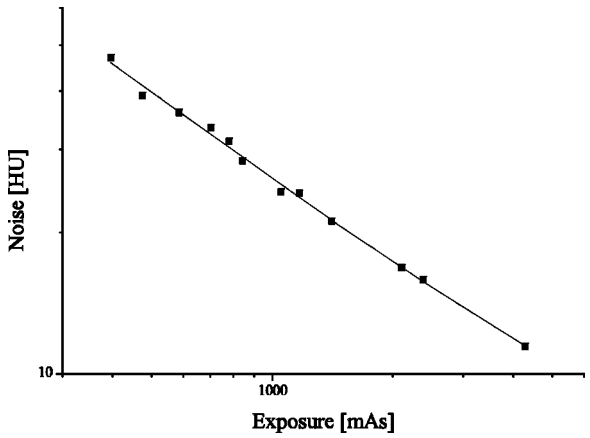

FIG. 3. Noise (standard deviation) of the signal in a homogeneous water phantom for 50 μm voxels is plotted as a function of exposure. A power-law fit with quadrature offset to the data is shown as a solid line.

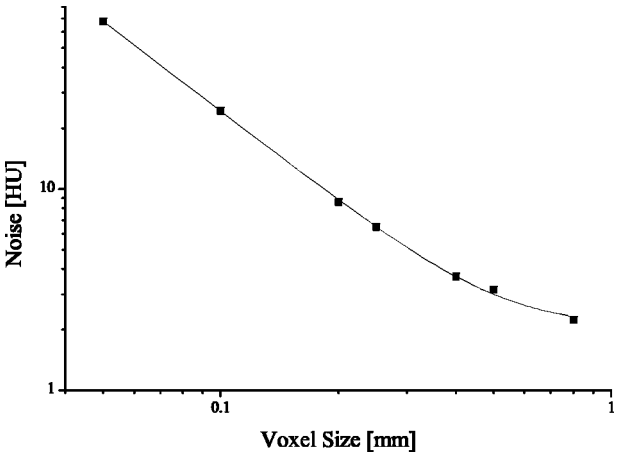

FIG. 4. Noise in a homogeneous water phantom as a function of voxel size at 119 mAs exposure. A power-law fit with quadrature offset to the data is shown as a solid line.

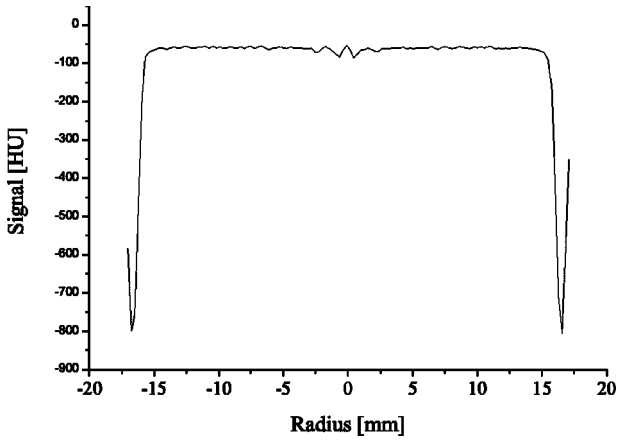

FIG. 6. Cross-sectional intensity profile of an acrylic disk in one axial plain reconstructed with 250 μm voxels.

profiles for a 25 μm aluminum wire are shown in Fig. 8(b). The absorption of aluminum is about 6500 HU as compared with 4000 HU for MICROFIL. As expected from the width of the PLSF, the width of the lateral profile of the aluminum wire is approximately 3 voxels and the same as for the MICROFIL-filled 18 μm tube. The peak intensity is higher and reaches 2500 HU.

(x) Figure 8(c) shows the lateral signal profiles of a 163 μm tube filled with MICROFIL, which is large compared to the width of the PLSF. However, the FWHM of the signal profiles is only about 9 voxels (98 μm) in the x direction and 11 voxels (119 μm) in the y direction. Using a threshold level of 800 HU, the diameter estimation would be 13 voxels (141 μm) in the x direction and 15 voxels (163 μm) in the y direction, which is closer to the true diameter. The peak on the left side of the profile in the x direction in Fig. 8(c) indicates that considerable settling of the contrast particles occurs. The peak location in the tubing is consistent with the direction of gravity during the solidification process. We have observed much stronger settling in larger vessels of up to 10 000 HU with MICROFIL.

(xi) Images of three different specimens are shown in Fig. 9. Figure 10 is a magnified rendering of the area marked by a box in Fig. 9(e). The reconstruction was executed using both processors of a Pentium III Dual Xeon 833 MHz PC with 1 GB of RAM. Experimental parameter, computation times, and the resulting contrast and noise values are summarized in Table I.

IV. DISCUSSION

The above results demonstrate the capabilities of microCT systems of this type. Potential microCT users will be able to make quantitative comparisons between this system and comparable systems manufactured by other companies like Imtek (Knoxville, TN), Scanco (Bassersdorf, Switzerland), SkyScan (Aartselaar, Belgium), and Stratec-Medizintechnik (Pforzheim, Germany), or research systems.

For high-contrast objects like contrast-filled vessels, the FWHM of the PLSF is a quantitative and intuitive measure of the smallest resolvable structure. While the resolution limit of the GE system was found to be 22 μm (FWHM of

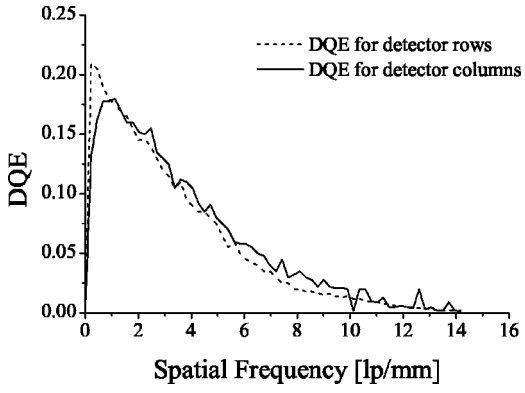

FIG. 5. Detected quantum efficiency (DQE) as a function of spatial frequency for the horizontal and vertical detector dimension computed by Cunningham from acceptance test data of an equivalent detector.

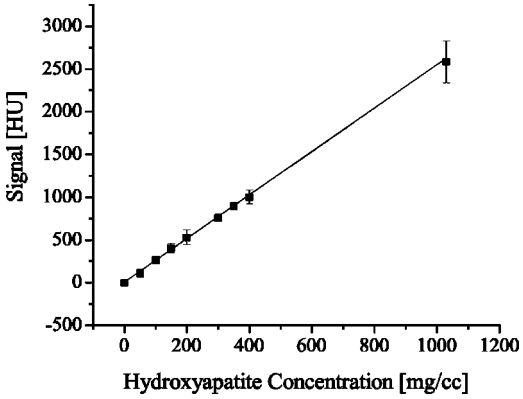

FIG. 7. Linear regression fit of the average intensity values in 20×20×20 voxel regions with 8 different hydroxyapatite concentrations.

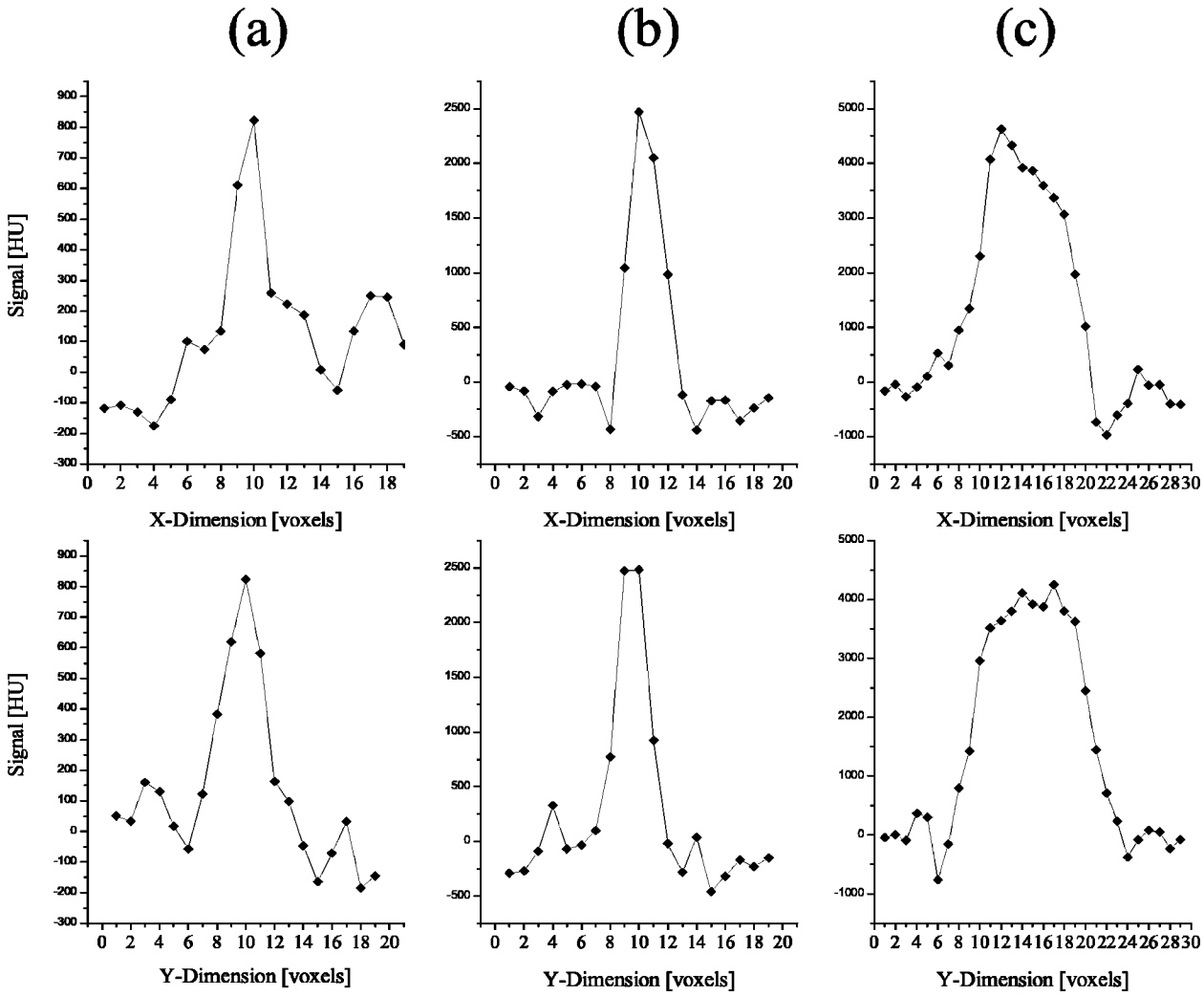

FIG. 8. Signal profiles in the two lateral directions (*X* and *Y*) of axially oriented PMMA tubes filled with MICROFIL and a 25 μm aluminum wire (b). The inner diameter of the PMMA tubes is 18 μm (a) and 162 μm (c). The voxel size is 10.85 μm.

PLSF), smaller structures of high contrast can certainly still be detected. Next to the 18 μm PMMA tube, we were also able to detect a 5 μm diameter tungsten wire embedded in epoxy resin with a contrast to noise ratio of 26 at a magnification of 3.2, a voxel size of 11 μm, and an exposure of 180 mAs (data not presented).

The noise behavior of the system is complicated and we did not attempt to model it. The measured exponents in the power laws of noise in HU as a function of exposure of -0.63 and as a function of voxel size of -1.49 (ignoring the offset) differ significantly from the expected values of -0.5 and -2 (Refs. 20, 21) for photon noise only. This indicates that other sources of noise are contributing. It should be noted that the noise at voxel sizes below 50 μm cannot be estimated from the given equation because of the necessary change in magnification.

The observed strong variations in contrast even within a single vessel and PMMA tubing [Fig. 8(c)] and between different vessels (Fig. 9) for all contract agents are a serious obstacle for the accurate determination of vessel diameter. Methods that rely on a rectangular cross-sectional contrast profile, like the FWHM or the area brightness product (ABP) method,[22] will be biased. We have shown that the FWHM underestimates the diameter of a tube with a diameter that is large compared to the PLSF. While wire phantom scans are useful for testing contrast sensitivity and system geometry, they may not be appropriate to test the accuracy of procedures to measure the diameter of contrast-filled vessels. By selecting a low threshold above the noise background (800 HU in experiment *x*), the diameter of a tube filled with MICROFIL could be determined with a precision of 2–3 pixels or the width of the PLSF. More precise measurements, for example using the fitting approach presented by Karau *et al.*,[23] will be difficult to perform and require knowledge about the contrast profile within the examined vessel.

Figures 9 and 10 demonstrate the wealth of information that can be obtained with microCT and are a qualitative comparison between three different contrast agents that have been used in our lab. While good results can be obtained with all of these agents, we currently use mainly MICROFIL in our lab because it is easy to handle, contrast particles do not settle as quickly as with Baritop, and the problem of

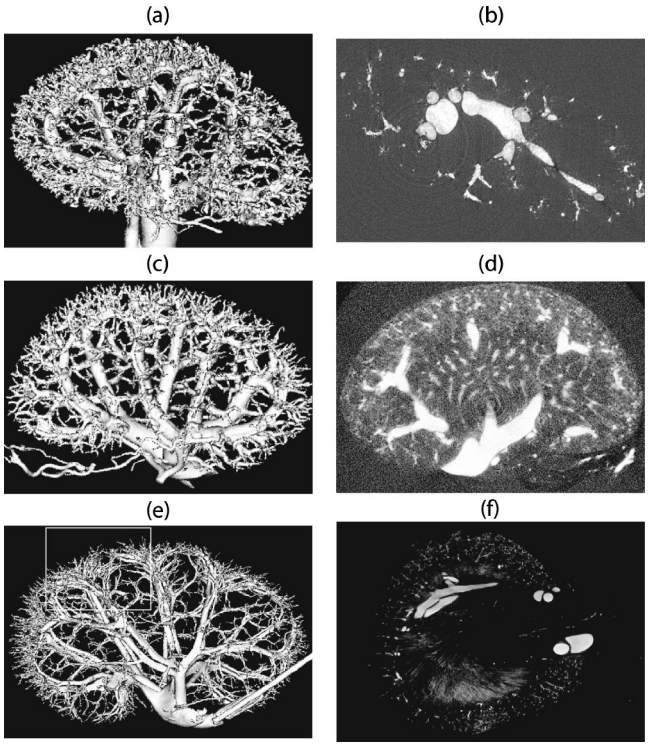

FIG. 9. Surface renderings (left) and central axial slices (right) of the reconstructed data of CT scans of a mouse kidney casted using Batson's No. 17 (a), (b), a fixed mouse kidney filled with MICROFIL (c), (d), and a rabbit kidney injected with Baritop contrast agent (e), (f). The FOV in (a), (b), (c), and (d) are approximately 10 mm and 37 mm in (e) and (f). The voxel sizes were 11 (b), (d) and 22 μm (f). Figure 10 is a higher resolution rendering of the region marked by a box in (e).

vessel loss due to breakage, that occurs with casting, is avoided. The dilutent for MICROFIL is also commercially available in two different viscosities. In this study, only the low-viscosity MICROFIL was used. Leakage of contrast into the kidney tubules and interstitial space was observed for both MICROFIL and Baritop [Figs. 9(d) and (f)]. Seeded region growing is effective in the segmentation of vessels to overcome this problem. Finally, the choice of contrast agent will depend on the application and investigator preference.

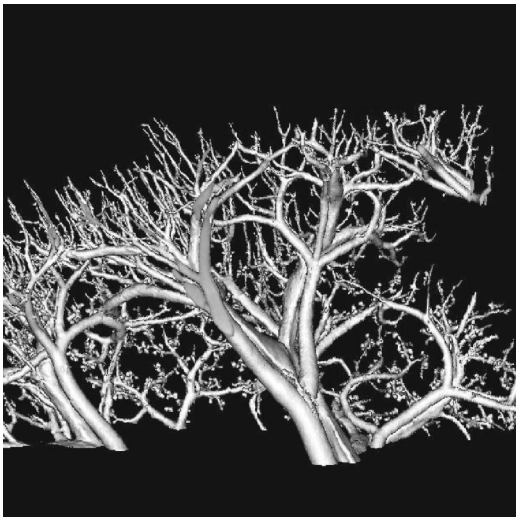

FIG. 10. Rendering of the area marked by a box in Fig. 9(e) using the full resolution (22 μm voxels) data set.

V. CONCLUSION

The performance of a high-resolution microCT was evaluated. It was shown that the system is well suited for the analysis of vascular structures. Vessels down to 22 μm in diameter can be resolved. The system allows convenient quantitative analysis of the morphology of vascular beds in tissue samples with a linear dimension up to 5 cm. Different contrast agents were discussed, all of which exhibit nonuniform intensity distributions. Imaging of PMMA tubing filled with MICROFIL proves that even vessels below 20 μm in diameter are detectable. Diameters can be estimated based on a low threshold value with a precision of 2–3 pixels. More precise estimates of vessel diameter will be difficult due to the nonuniformity of vessel contrast.

ACKNOWLEDGMENTS

The authors would like to thank Allan Seifert and Michael J. Flynn for providing the ruby sphere resolution phantom and assistance with data processing. We would also like to thank Hao Lai and Ian Cunningham for the analysis of the DQE data as well as James Mainprize for providing code to calculate the detector MTF. This work was supported by the Canadian Institutes of Health Research.

[1] D. A. Beard and J. B. Bassingthwaighte, "Fractal nature of myocardial blood flow emerges from whole-organ model of arterial network," J. Vasc. Res. **37**, 282–296 (2000).
[2] G. M. J. van Leeuwen, A. N. T. J. Kotte, and J. J. J. W. Lagendijk, "A flexible algorithm for construction of 3D vessel networks for use in thermal modeling," IEEE Trans. Biomed. Eng. **45**, 596–604 (1998).
[3] R. Turner, "How much cortex can a vein drain? Downstream dilution of activation-related cerebral blood oxygenation changes," Neuroimage **16**, 1062–1067 (2002).
[4] J. Folkman, "New perspectives in clinical oncology from angiogenesis research," Eur. J. Cancer **32A**, 2534–2539 (1996).
[5] L. A. Feldkamp, L. C. Davis, and J. W. Kress, "Practical cone-beam algorithm," J. Opt. Soc. Am. A **1**, 612–619 (1984).
[6] S. M. Jorgensen, O. Demirkaya, and E. L. Ritman, "Three-dimensional imaging of vasculature and parenchyma in intact rodent organs with x-ray micro-CT," Am. J. Physiol. Heart Circ. **44**, H1103–H1114 (1998).
[7] E. Toyota, K. Fujimoto, Y. Ogasawara, T. Kajita, F. Shigeto, T. Matsumoto, M. Goto, and F. Kajiya, "Dynamic changes in three-dimensional architecture and vascular volume of transmural coronary microvasculature between diastolic- and systolic-arrested rat hearts," Circulation **105**, 621–626 (2002).
[8] K. L. Karau, R. C. Molthen, A. Dhyani, S. T. Haworth, C. C. Hanger, D. L. Roerig, R. H. Johnson, and C. A. Dawson, "Pulmonary arterial morphometry from microfocal x-ray computed tomography," Am. J. Physiol. Heart Circ. **281**, H2747–H2756 (2001).
[9] M. A. Konerding, A. J. Miodonski, and A. Lametschwandtner, "Microvascular corrosion casting in the study of tumor vascularity: A review," Scanning Microsc. **9**, 1233–1244 (1995).
[10] M. Zamir and P. Sinclair, "Roots and calibers of the human coronary arteries," Am. J. Anat. **183**, 226–234 (1988).
[11] E. Kaczmarek and R. L. Becker, Jr., "Three-dimensional modeling of renal glomerular capillary networks," Anal Quant Cytol. Histol. **19**(2), 93–101 (1997).
[12] P. A. Kay, R. A. Robb, and D. G. Bostwick, "Prostate cancer microvessels: A novel method for three-dimensional reconstruction and analysis," Prostate **37**, 270–277 (1998).

[13] "Regulations respecting X-Ray Safety—made under the Occupational Health and Safety Act," Ontario Ministry of Labour (1980).
[14] G. N. Ramachandran and A. V. Lakshminarayanan, "Three-dimensional reconstruction form radiographs and electron micrographs: Application of convolutions instead of Fourier transforms," Proc. Natl. Acad. Sci. U.S.A. **68**, 2236–2240 (1971).
[15] D. L. Parker, "Optimal short scan convolution reconstruction for fan-beam CT," Med. Phys. **9**, 254–257 (1982).
[16] A. Seifert and M. J. Flynn, "Resolving power of 3D x-ray microtomography systems," Proc. SPIE **4682**, 407–413 (2002).
[17] J. H. Siewerdsen, L. E. Antonuk, Y. El-Mohri, J. Yorkston, W. Huang, and I. A. Cunningham, "Signal, noise power spectrum, and detective quantum efficiency of indirect-detection flat-panel imagers for diagnostic radiology," Med. Phys. **25**(5), 614–628 (1998).
[18] B. J. Gannon, "Vascular casting," in *Principles and Techniques of Scanning Electron Microscopy*, edited by M. A. Hayat (Van Nostrand Reinhold, New York, 1974), p. 170.
[19] K. Sugimoto, N. Sakurai, M. Kaneko, H. Shirasawa, K. Shibata, M. Miyata, T. No, K. Uematsu, K. Shimoda, and J. Sakata, "Application of renal microangiography to normal and diseased kidneys of cattle and mice," Am. J. Vet. Res. **52**, 157–163 (1991).
[20] J. C. Gore and P. S. Tofts, "Statistical limitation in computed tomography," Phys. Med. Biol. **23**, 1176–1182 (1978).
[21] R. A. Brooks and G. Di Chiro, "Statistical limitations in x-ray reconstructive tomography," Med. Phys. **3**(4), 237–240 (1976).
[22] M. Block, Y.-H. Liu, L. D. Harris, R. A. Robb, and E. L. Ritman, "Quantitative analysis of a vascular tree model with the dynamic spatial reconstructor," J. Comput. Assist. Tomogr. **8**(3), 390–400 (1984).
[23] K. L. Karau, R. H. Johnson, R. C. Molthen, A. H. Dhyani, S. T. Haworth, C. C. Hanger, D. L. Roerig, and C. A. Dawson, "Microfocal x-ray CT imaging and pulmonary arterial distensibility in excised rat lungs," Am. J. Physiol. Heart Circ. Physiol. **281**, 1447–H1457 (2001).